Article

Spectroscopic Studies of the Interaction of Ferrous Bleomycin with DNA

Jyllian N. Kemsley, Kelly Loeb Zaleski, Marina S. Chow, Andrea Decker, Ekaterina Y. Shishova, Erik C. Wasinger, Britt Hedman, Keith O. Hodgson, and Edward I. Solomon

J. Am. Chem. Soc., **2003**, 125 (36), 10810-10821• DOI: 10.1021/ja034579n • Publication Date (Web): 15 August 2003

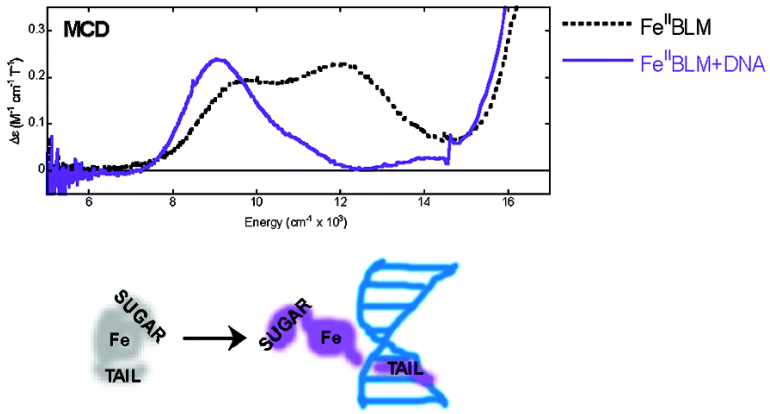

More About This Article

Additional resources and features associated with this article are available within the HTML version:

- Supporting Information
- Links to the 1 articles that cite this article, as of the time of this article download
- Access to high resolution figures
- Links to articles and content related to this article
- Copyright permission to reproduce figures and/or text from this article

View the Full Text HTML

J|A|C|S
ARTICLES
Published on Web 08/15/2003

Spectroscopic Studies of the Interaction of Ferrous Bleomycin with DNA

Jyllian N. Kemsley,[†] Kelly Loeb Zaleski,[†] Marina S. Chow,[†] Andrea Decker,[†] Ekaterina Y. Shishova,[†] Erik C. Wasinger,[†] Britt Hedman,*[,§] Keith O. Hodgson,*[,†,§] and Edward I. Solomon*[,†]

Contribution from the Department of Chemistry, Stanford University, Stanford, California 94305, and Stanford Synchrotron Radiation Laboratory, SLAC, Stanford University, Stanford, California 94309

Received February 10, 2003; E-mail: edward.soloman@stanford.edu; hodgson@ssrl.slac.standford.edu; hedman@ssrl.slac.stanford.edu

Abstract: Bleomycin is an antibiotic used in cancer chemotherapy for its ability to achieve both single- and double-strand cleavage of DNA through abstraction of the deoxyribose C4′−H. Magnetic circular dichroism (MCD) and X-ray absorption (XAS) spectroscopies have been used to study the interaction of the biologically relevant Fe^{II}BLM complex with DNA. Calf thymus DNA was used as the substrate as well as short oligonucleotides, including one with a preferred 5′-G-pyrimidine-3′ cleavage site [d(GGAAGCTTCC)$_2$] and one without [d(GGAAATTTCC)$_2$]. DNA binding to Fe^{II}BLM significantly perturbs the Fe^{II} active site, resulting in a change in intensity ratio of the d → d transitions and a decrease in excited-state orbital splitting (Δ^5E_g). Although this effect is somewhat dependent on length and composition of the oligonucleotide, it is *not* correlated to the presence of a 5′-G-pyrimidine-3′ cleavage site. No effect is observed on the charge-transfer transitions, indicating that the H-bonding recognition between the pyrimidine and guanine base does not perturb Fe−pyrimidine backbonding. Azide binding studies indicate that Fe^{II}BLM bound to either oligomer has the same affinity for N_3^-. Parallel studies of BLM structural derivatives indicate that Fe^{II}*iso*-PEPLM, in which the carbamoyl group is shifted on the mannose sugar, forms the same DNA-bound species as Fe^{II}BLM. In contrast, Fe^{II}DP-PEPLM, in which the β-aminoalanine group is absent, forms a new species upon DNA binding. These data are consistent with a model in which the primary amine from the β-aminoalanine is an Fe^{II} ligand and the mannose carbamoyl provides either a ligand to the Fe^{II} or significant second-sphere effects on the Fe^{II} site; intercalation of the bithiazole tail into the double helix likely brings the metal-bound complex close enough to the DNA to create steric interactions that remove the sugar groups from interaction with the Fe^{II}. The fact that the Fe^{II} active site is perturbed regardless of DNA sequence is consistent with the fact that cleavage is observed for both 5′-GC-3′ and nonspecific oligomers and indicates that different reaction coordinates may be active, depending on orientation of the deoxyribose C4′-H.

1. Introduction

Bleomycins (BLMs)[1] are antitumor antibiotics used to treat head and neck cancer, Hodgkin's disease, and testicular cancer. First characterized in the 1960s,[2] they are believed to act therapeutically by binding to and cleaving DNA in the presence of a metal ion. Although BLM is isolated from *Streptomyces verticillus* as a Cu complex, it is administered clinically in a metal-free form. The active species in vivo is believed to be Fe^{II}BLM.[3]

Fe^{II}BLM reacts with oxygen to produce selective single- and double-strand cleavage of DNA and RNA.[4−7] Oxygen binds to Fe^{II}BLM to produce the "oxygenated" species, formally an Fe^{III}−superoxide complex,[8,9] which then accepts an additional electron, either in a disproportionation reaction or through another reductant, to form "activated" BLM, a low-spin Fe^{III}−hydroperoxide complex.[9−16] Activated BLM is the last intermediate that has been detected prior to initiating DNA

[†] Department of Chemistry, Stanford University.
[§] Stanford Synchrotron Radiation Laboratory.

(1) Abbreviations: BLM, bleomycin; CD, circular dichroism; ctDNA, calf thymus DNA.; DNA_{GC}, d(GGAAGCTTCC)$_2$; DNA_{ns}, d(GGAAATTTCC)$_2$; DP-PEPLM, depyruvamide peplomycin derivative; Fe^{II}AS, ferrous ammonium sulfate; ENDOR, electron nuclear double resonance; EPR, electron paramagnetic resonance; EXAFS, extended X-ray absorption fine structure; Im, imidazole; *iso*-PEPLM, *iso*-pepleomycin derivative; MCD, magnetic circular dichroism; PEPLM, peplomycin; TMC, 1,4,8,11-tetramethyl-1,4,-8,11-tetraazacyclotetradecane; VTVH, variable-temperature variable-field; XAS, X-ray absorption spectroscopy; ZFS, zero-field splitting; 4C, four-coordinate; 5C, five-coordinate; 6C, six-coordinate.

(2) Umezawa, H. *GANN Monogr. Cancer Res.* **1976**, *19*, 3−36.
(3) Radtke, K.; Lornitzo, F. A.; Byrnes, R. W.; Antholine, W. E.; Petering, D. H. *Biochem. J.* **1994**, *302*, 655−664.
(4) Petering, D. H.; Mao, Q.; Li, W.; DeRose, E.; Antholine, W. E. In *Probing of Nucleic Acids by Metal Ion Complexes of Small Molecules*; Sigel, A., Sigel, H., Eds.; Marcel Dekker: New York, 1996; Vol. 33, pp 619−648.
(5) Stubbe, J.; Kozarich, J. W.; Wu, W.; Vanderwall, D. E. *Acc. Chem. Res.* **1996**, *29*, 322−330.
(6) Burger, R. M. *Chem. Rev.* **1998**, *98*, 1153−1169.
(7) Hecht, S. M. *J. Nat. Prod.* **2000**, *63*, 158−168.
(8) Burger, R. M.; Horwitz, S. B.; Peisach, J.; Wittenberg, J. B. *J. Biol. Chem.* **1979**, *254*, 12299−12302.
(9) Burger, R. M.; Kent, T. A.; Horwitz, S. B.; Münck, E.; Peisach, J. *J. Biol. Chem.* **1983**, *258*, 1559−1564.
(10) Burger, R. M.; Peisach, J.; Horwitz, S. B. *J. Biol. Chem.* **1981**, *256*, 11636−11644.

10.1021/ja034579n CCC: $25.00

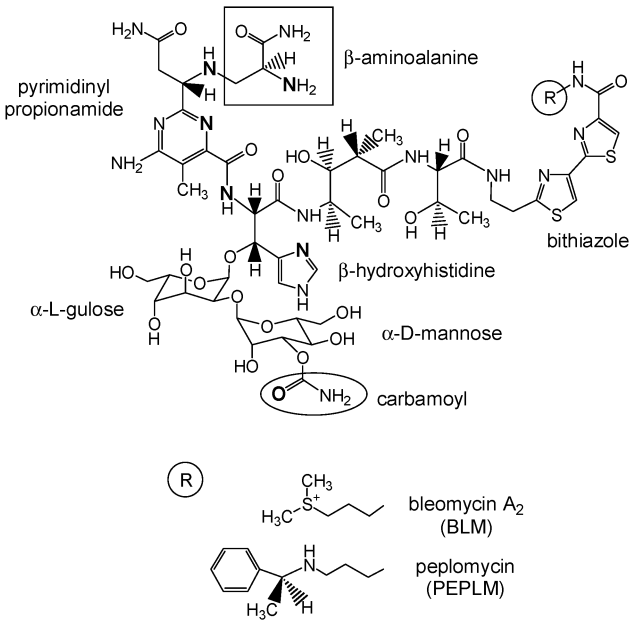

Figure 1. BLM ligand structure.

strand scission by abstracting the C4′−H from a deoxyribose sugar.[17] This produces a C4′ radical on the sugar; the DNA then cleaves through two possible pathways depending on O_2 availability.[18−20] Given the $\sim 10^5$ M^{-1} binding constant for BLM to DNA, it is likely that Fe^{II}BLM is bound to DNA before becoming activated.[4,21]

BLM is typically described as having three functional domains (Figure 1): the bithiazole tail, which intercalates into the DNA double helix; the sugar moiety, believed to be involved in drug uptake into cells; and the β-aminoalanine, pyrimidine, and β-hydroxyhistidine groups, collectively known as the metal-binding region. The three-dimensional structure of BLM has been interpreted from the crystal structures of the Cu^{II} complex of the BLM synthetic precursor P-3A,[22] and model complexes with Cu^{II},[23,24] Co^{III},[25,26] and Zn^{II}.[27] NMR studies and molecular dynamics modeling have also been conducted on the Zn^{II}, Cd^{II}, Fe^{II}, Fe^{II}−CO, Co^{III}, and Co^{III}−OOH complexes,[21,28−31] some on BLM derivatives and/or with a bound oligonucleotide. The only crystal structure available for the complete BLM molecule is one in which Cu^{II}BLM is bound to a BLM-resistance protein from *S. verticillus*.[32] It should be noted that of the close to three dozen structural studies done for BLM, only one has investigated the catalytically relevant Fe^{II} drug complex.[33]

Possible metal ligands are shown in bold in Figure 1. It is generally accepted that the four equatorial ligands are an imidazole nitrogen and the deprotonated amide of the β-hydroxyhistidine, a pyrimidine nitrogen, and the secondary amine of the β-aminoalanine fragment. The identity of the axial ligands remains controversial, with various groups proposing five endogenous ligands with either the primary amine of the β-aminoalanine *or* the mannose carbamoyl as a ligand, along with solvent at the sixth site, or six endogenous ligands with *both* the primary amine and carbamoyl bound to the metal. Additionally, structures vary depending on the screw sense produced by how the ligand wraps around the metal. One orientation has both the β-aminoalanine and sugars on the same side of the equatorial plane, while the other allows them to be on opposite sides of the metal. (See references in previous paragraph.)

The bithiazole tail binds nonspecifically to the DNA via partial intercalation into the DNA double helix. BLM cleaves preferentially at 5′-GC-3′ or 5′-GT-3′ sequences; that specificity is conferred by the metal-binding domain, primarily through hydrogen-bonding interactions between the BLM pyrimidine and the DNA guanine.[34−36] The bulk of the $\sim 10^5$ M^{-1} binding constant for BLM binding to DNA is provided by bithiazole tail intercalation, with the sequence-specific interaction of the metal-binding domain contributing a small additional amount.[37]

Several studies have demonstrated interactions between the metal-binding domain of the drug with DNA. Fe^{III}BLM is low spin at high pH but goes high spin at low pH; binding to DNA returns the complex to a low-spin species (at low pH).[38] Binding of exogenous ligands such as phosphate and azide to Fe^{III}BLM is also reversed upon DNA binding.[10,38] The oxygenated species ($^{-\bullet}O_2$−Fe^{III}BLM) is stabilized when bound to DNA, primarily because the complexes are less accessible for the disproportionation reaction.[39−41] The electron paramagnetic resonance (EPR) spectrum of ON−Fe^{II}BLM is rhombically perturbed in

(11) Kuramochi, H.; Takahashi, K.; Takita, T.; Umezawa, H. *J. Antibiot.* **1981**, *34*, 576−582.
(12) Sam, J. W.; Tang, X.-J.; Peisach, J. *J. Am. Chem. Soc.* **1994**, *116*, 5250−5256.
(13) Burger, R. M.; Tian, G.; Drlica, K. *J. Am. Chem. Soc.* **1995**, *117*, 1167−1168.
(14) Veselov, A.; Sun, H.; Sienkiewicz, A.; Taylor, H.; Burger, R. M.; Scholes, C. P. *J. Am. Chem. Soc.* **1995**, *117*, 7508−7512.
(15) Westre, T. E.; Loeb, K. E.; Zaleski, J. M.; Hedman, B.; Hodgson, K. O.; Solomon, E. I. *J. Am. Chem. Soc.* **1995**, *117*, 1309−1313.
(16) Burger, R. M. *Struct. Bonding* **2000**, *97*, 287−303.
(17) Sugiyama, H.; Ohmori, K.; Saito, I. *J. Am. Chem. Soc.* **1994**, *116*, 6, 10326−10327.
(18) Haidle, C. W.; Weiss, K. K.; Kuo, M. T. *Mol. Pharmacol.* **1972**, *8*, 531−537.
(19) Povirk, L. F.; Wübker, W.; Köhnlein, W.; Hutchinson, F. *Nucleic Acids Res.* **1977**, *4*, 3573−3580.
(20) Giloni, L.; Takeshita, M.; Johnson, F.; Iden, C.; Grollman, A. P. *J. Biol. Chem.* **1981**, *256*, 8608−8615.
(21) Claussen, C. A.; Long, E. C. *Chem. Rev.* **1999**, *99*, 2797−2816.
(22) Iitaka, Y.; Nakamura, H.; Nakatani, T.; Muraoka, Y.; Fujii, A.; Takita, T.; Umezawa, H. *J. Antiobiot.* **1978**, *31*, 1070−1072.
(23) Brown, S. J.; Tao, X.; Wark, T. A.; Stephan, D. W.; Mascharak, P. K. *Inorg. Chem.* **1988**, *27*, 1581−1587.
(24) Kurosaki, H.; Hayashi, K.; Ishikawa, Y.; Goto, M.; Inada, K.; Taniguchi, I.; Shionoya, M.; Kimura, E. *Inorg. Chem.* **1999**, *38*, 2824−2832.
(25) Tan, J. D.; Hudson, S. E.; Brown, S. J.; Olmstead, M. M.; Mascharak, P. K. *J. Am. Chem. Soc.* **1992**, *114*, 3841−3853.
(26) Farinas, E.; Tan, J. D.; Baidya, N.; Mascharak, P. K. *J. Am. Chem. Soc.* **1993**, *115*, 2996−2997.
(27) Kurosaki, H.; Hayashi, K.; Ishikawa, Y.; Goto, M. *Chem. Lett.* **1995**, 691−692.
(28) Lehmann, T. E.; Serrano, M. L.; Que, L., Jr. *Biochemistry* **2000**, *39*, 3886−3898.
(29) Hoehn, S. T.; Junker, H.-D.; Bunt, R. C.; Turner, C. J.; Stubbe, J. *Biochemistry* **2001**, *40*, 5894−5905.
(30) Lehmann, T. E. *J. Biol. Inorg. Chem.* **2002**, *7*, 305−312.
(31) Zhao, C.; Xia, C.; Mao, Q.; Försterling, H.; DeRose, E.; Antholine, W. E.; Subczynski, W. K.; Petering, D. H. *J. Inorg. Biochem.* **2002**, *91*, 259−268.
(32) Sugiyama, M.; Kumagai, T.; Hayashida, M.; Maruyama, M.; Matoba, Y. *J. Biol. Chem.* **2002**, *277*, 2311−2320.
(33) Lehmann, T. E.; Ming, L.-J.; Rosen, M. E.; Que, L., Jr. *Biochemistry* **1997**, *36*, 2807−2816.
(34) Wu, W.; Vanderwall, D. E.; Turner, C. J.; Kozarich, J. W.; Stubbe, J. *J. Am. Chem. Soc.* **1996**, *118*, 1281−1294.
(35) Vanderwall, D. E.; Lui, S. M.; Wu, W.; Turner, C. J.; Kozarich, J. W.; Stubbe, J. *Chem. Biol.* **1997**, *4*, 373−387.
(36) Boger, D. L.; Ramsey, T. M.; Cai, H.; Hoehn, S. T.; Kozarich, J. W.; Stubbe, J. *J. Am. Chem. Soc.* **1998**, *120*, 53−65.
(37) Li, W.; Zhao, C.; Xia, C.; Antholine, W. E.; Petering, D. H. *Biochemistry* **2001**, *40*, 7559−7568.
(38) Albertini, J. P.; Garnier-Suillerot, A. *Biochemistry* **1984**, *23*, 47−53.
(39) Burger, R. M.; Peisach, J.; Blumberg, W. E.; Horwitz, S. B. *J. Biol. Chem.* **1979**, *254*, 10906−10912.
(40) Albertini, J.-P.; Garnier-Suillerot, A.; Tosi, L. *Biochem. Biophys. Res. Commun.* **1982**, *104*, 557−563.
(41) Fulmer, P.; Petering, D. H. *Biochemistry* **1994**, *33*, 5319−5327.

the presence of DNA.[42−44] Several of these effects have been correlated with the 5′-GC-3′ cleavage site.[45,46] Additionally, Fe^{III}BLM and HOO−Co^{III}BLM bind to oligonucleotides with a preferred cleavage site in slow exchange on the NMR time scale but in fast exchange to oligomers without preferred cleavage sites.[37,47] Sequence-specific perturbations of the EPR and resonance Raman spectra of low-spin Fe^{III}BLM have been correlated with a reduction in possible conformers of the drug complex.[48] Changes in Fe^{III}BLM features observed by Q-band electron nuclear double resonance (ENDOR) were interpreted as consistent with a better-defined structure in the presence of calf thymus DNA and a GC-containing nucleotide, although the hyperfine couplings of first-shell ligands were unchanged.[49] Experiments with oligonucleotides have indicated that Fe^{III}BLM, when reacted with ascorbate and O_2, produces DNA cleavage products at a *faster* rate when a preferred cleavage site is *not* present.[45]

To investigate Fe^{II}BLM, the catalytically active form in vivo, we have employed circular dichroism (CD), magnetic CD (MCD), and X-ray absorption spectroscopy (XAS). In particular, we have developed variable-temperature, variable-field (VTVH) MCD as a powerful probe of the catalytically relevant ferrous form of non-heme iron systems. XAS provides an important complement to the MCD methodology in that the preedge can also probe coordination number while the extended X-ray absorption fine structure (EXAFS) provides metal−ligand bond lengths.

Our previous studies demonstrated that the resting Fe^{II}BLM active site is six-coordinate (6C) with a distorted octahedral geometry and one weak axial ligand.[50] A short Fe−pyrimidine bond distance of 2.06 Å combined with the presence of low-energy charge-transfer transitions were attributed to $d_\pi \rightarrow$ pyrimidine π^* back-bonding in the equatorial plane, which contributes to the unique stability of the oxygenated and activated species in a non-heme ligand environment.[50]

Expansion of these studies to investigate selected BLM structural derivatives indicated that differences in the bithiazole C-substituent have no effect on the metal atom; however, perturbations of the β-aminoalanine fragment and the mannose carbamoyl moiety produce significant effects on the Fe^{II} site.[51,52] Effects observed in the mannose sugar derivatives included a decrease in energy of the excited-state orbitals and increased ground-state orbital splitting; an increase in the Fe−pyrimidine bond length was correlated to a decrease in intensity of the metal-to-ligand charge-transfer transitions. Removing the β-aminoalanine fragment resulted in increased splittings of *both* the excited- and ground-state orbitals, and a significantly longer Fe−pyrimidine bond was consistent with a shift in charge-transfer transitions to higher energy (reduced back-bonding) and further decreased intensity. Reduced azide-binding affinities in the derivatives correlated with their reduced DNA cleavage capability.[53−58] These results demonstrated that the primary amine of the β-aminoalanine is an Fe^{II} ligand, and the carbamoyl either provides a sixth endogenous ligand or contributes significantly to the coordination environment of the Fe^{II} site through second-sphere effects.

We now extend these studies further to investigate the interaction of Fe^{II}BLM with calf-thymus DNA (ctDNA) and selected oligonucleotides, with and without a preferred 5′-GC-3′ cleavage site, whose reactivity and selectivity have been extensively studied by others.[31,37,45−47] We again employ the use of BLM structural derivatives to probe the composition of ligands to the Fe^{II} site and their role in DNA binding. The results from this study provide new insight into the Fe^{II}BLM interaction with DNA and its reactivity with O_2.

2. Materials and Methods

2.1. Chemicals. All commercial reagents were of the highest grade available and were used without further purification. Metal-free bleomycin sulfate, calf thymus DNA, and HEPES were purchased from Sigma Chemical Co. (now Sigma-Aldrich Corp.). The bleomycin derivatives *iso*-peplomycin and DP-peplomycin were obtained from Nippon Kayaku Co. (Tokyo, Japan). DNA oligonucleotides were obtained from QUIAGEN Operon (Alameda, CA) or the PAN Facility (Beckman Center, Stanford University), or as a gift from Professor Sidney Hecht (University of Virginia). All spectra were from samples prepared with HPLC-purified oligomers from Operon unless otherwise noted in the caption. To achieve the necessary concentrations, several 1 μmol syntheses were ordered, and aliquots were combined and lyophilized at the Operon facility. D_2O and NaOD (99.9 atom % D) as well as NaN_3 were obtained from Aldrich (now Sigma-Aldrich Corp.). Glycerol-d_3 (98 atom % D) was obtained from Cambridge Isotopes Laboratories. $Fe(NH_4)_2(SO_4)_2 \cdot 6H_2O$ (Fe^{II}AS) was from MCB Manufacturing Chemists. NO gas (98.5%) was purchased from Aldrich (now Sigma-Aldrich Corp.).

2.2. Sample Preparation. Strictly anaerobic conditions were maintained throughout sample preparation as the use of reducing agents such as dithionite have been determined to affect the CD and MCD features of Fe^{II}BLM. HEPES buffer was prepared in D_2O and adjusted to pD 8.2 with NaOD. Buffer solution, D_2O, and glycerol-d_3 were degassed with 10−20 freeze−pump−thaw cycles at 10^{-3} Torr in Teflon- and ground glass-stoppered flasks. Calf thymus DNA (ctDNA), DNA oligomers, Fe^{II}AS, and NaN_3 were purged under Ar for 2−3 h in vials capped with rubber stoppers. Bleomycin and its derivatives were evacuated and filled with Ar ~20 times in Teflon-capped conical vials. Once degassing/purging was complete, all materials were immediately transferred into an N_2 atmosphere glovebox (<10 ppm O_2).

(42) Antholine, W. E.; Petering, D. H. *Biochem. Biophys. Res. Commun.* **1979**, *91*, 528−533.
(43) Sugiura, Y.; Ishizu, K. *J. Inorg. Biochem.* **1979**, *11*, 171−180.
(44) Kennedy, M. C.; Antholine, W. E.; Li, W.; Mao, Q.; Petering, D. H. *Inorg. Chim. Acta* **1995**, *240*, 535−540.
(45) Fulmer, P.; Zhao, C.; Li, W.; DeRose, E.; Antholine, W. E.; Petering, D. H. *Biochemistry* **1997**, *36*, 4367−4374.
(46) Li, W.; Xia, C.; Antholine, W. E.; Petering, D. H. *J. Biol. Inorg. Chem.* **2001**, *6*, 618−627.
(47) Mao, Q.; Fulmer, P.; Li, W.; DeRose, E. F.; Petering, D. H. *J. Biol. Chem.* **1996**, *271*, 6185−6191.
(48) Sam, J. W.; Takahashi, S.; Lippai, I.; Peisach, J.; Rousseau, D. L. *J. Biol. Chem.* **1998**, *273*, 16090−16097.
(49) Veselov, A.; Burger, R. M.; Scholes, C. P. *J. Am. Chem. Soc.* **1998**, *120*, 1030−1033.
(50) Loeb, K. E.; Zaleski, J. M.; Westre, T. E.; Guajardo, R. J.; Mascharak, P. K.; Hedman, B.; Hodgson, K. O.; Solomon, E. I. *J. Am. Chem. Soc.* **1995**, *117*, 4545−4561.
(51) Loeb, K. E.; Zaleski, J. M.; Hess, C. D.; Hecht, S. M.; Solomon, E. I. *J. Am. Chem. Soc.* **1998**, *120*, 1249−1259.
(52) Wasinger, E. C.; Loeb Zaleski, K.; Hedman, B.; Hodgson, K. O.; Solomon, E. I. *J. Biol. Inorg. Chem.* **2002**, *7*, 157−164.
(53) Takahashi, K.; Ekimoto, H.; Aoyagi, S.; Koyu, A.; Kuramochi, H.; Yoshioka, O.; Matsuda, A.; Fujii, A.; Umezawa, H. *J. Antiobiot.* **1979**, *32*, 36−42.
(54) Ehrenfeld, G. M.; Murugesan, M.; Hecht, S. M. *Inorg. Chem.* **1984**, *23*, 1496−1498.
(55) Sugiyama, H.; Kilkuskie, R. E.; Chang, L.-H.; Ma, L.-T.; Hecht, S. M.; van der Marel, G. A.; van Boom, J. H. *J. Am. Chem. Soc.* **1986**, *108*, 3852−3854.
(56) Shipley, J. B.; Hecht, S. M. *Chem. Res. Toxicol.* **1988**, *1*, 25−27.
(57) Boger, D. L.; Teramoto, S.; Honda, T.; Zhou, J. *J. Am. Chem. Soc.* **1995**, *117*, 7338−7343.
(58) Boger, D. L.; Teramoto, S.; Zhou, J. *J. Am. Chem. Soc.* **1995**, *117*, 7344−7356.

In the glovebox, HEPES buffer was first used to solvate the DNA. In the case of small oligonucleotides obtained from Operon, the vial was then placed for 3 min in a sand bath maintained at 90 °C and subsequently allowed to cool to room temperature to enable DNA duplex annealing. Fe^{II}AS and bleomycin were dissolved in D_2O and HEPES buffer, respectively. A small amount of Fe^{II}AS was then added to the bleomycin solution to generate the red/pink Fe^{II}BLM species, which was added to the DNA solution(s) and mixed thoroughly. To facilitate glassing in MCD samples, glycerol-d_3 was then added to make a 50% (v/v) solution. The same sample preparation protocol was followed for the bleomycin derivatives. Final sample concentrations were 1−2 mM Fe for calf thymus DNA samples and 3−4 mM Fe for oligonucleotide samples. Ratios of Fe^{II}:BLM:oligomer duplex were approximately 0.8:0.9:1.0 to ensure complete binding of metal to drug, and drug to oligomer.

For NO studies, pre-prepared Fe^{II}BLM and Fe^{II}BLM+DNA samples were transferred into an N_2-purged glovebag. NO gas, which was passed first through a 1 M NaOH drying solution and deionized H_2O, was blown into the headspace of a septum-sealed conical vial at room temperature. The sample was shaken periodically to ensure proper mixing. The red/pink color of Fe^{II}BLM darkened within a couple of minutes to a deep pink color, which quickly dissipated as the solution turned to a light yellow/orange color. The reaction was continued until there was no additional development of the yellow color, usually within 15 min. Samples were then transferred back to the glovebox for loading into EPR tubes.

For azide binding studies, degassed D_2O was added to Ar-purged NaN_3 in the glovebox. Azide was added to already prepared Fe^{II}BLM + DNA solutions, and the samples were mixed thoroughly.

Immediately upon preparation, samples for CD were injected into a 1 cm path length Infrasil quartz cuvette (Wilmad) adapted with a ChemGlass stopcock to prevent air oxidation during the time course of the experiment. MCD samples were injected into an MCD cell assembled with a neoprene spacer (0.3 cm path length) sandwiched between two Infrasil quartz disks (Heraeus Amersil or Esco Products) and stabilized between two fitted copper plates. Samples for EPR were loaded into EPR tubes. XAS samples were syringed into a 23 mm × 1 mm × 3 mm Lucite XAS cell with 37 μm Kapton windows. All samples were then quickly frozen in liquid N_2 and stored in the same until inserted into the cryostat under high flow of He gas.

2.3. CD and MCD Spectroscopy. Near-IR CD spectra (600−2000 nm) were obtained using a Jasco J200-D spectropolarimeter with a liquid N_2-cooled InSb detector. Spectra in the visible/UV range (300−800 nm) were obtained using a Jasco J810 spectropolarimeter with an extended S-20 photomultiplier tube. Data acquisition was achieved on the J200-D by using routines written within the software package LabVIEW (National Instruments) and on the J810 by using the Jasco Spectra Manager program. Contributions to the CD intensity due to buffer and cell backgrounds were subtracted from the protein CD spectra. CD spectra of Fe^{II}BLM+DNA with and without glycerol-d_3 are similar to CD spectra of Fe^{II}BLM; glycerol has no effect on the Fe^{II} active site (see Supporting Information, Figures S1 and S2).

Low-temperature MCD spectra (1.6−50 K) were obtained using the Jasco spectropolarimeters and an Oxford Instruments SM4000-7T or SM4-7T superconducting magnets/cryostats suspended in the beam path. Depolarization of frozen samples was monitored by measuring the differential CD intensity of a nickel (+)-tartarate solution placed before and after the sample compartment.[59] It should be noted that a significant amount of depolarization was observed in samples with high concentrations of ctDNA, perhaps because the large polymer strands and high sample viscosity affect the quality of the glass. This effect is wavelength dependent and might manifest itself in slightly altered band energies and intensities.

MCD spectra were corrected for zero-field baseline effects induced by variability in glass quality by subtracting off the corresponding 0 T scans at each temperature. Alternatively, the directionality of the applied magnetic field was reversed and the subtracted average of the +7 T and −7 T scans, [7 − (−7)]/2 T, was used. VTVH MCD data were collected at fixed temperatures of 1.5−1.7, 2.0−2.1, 3, 5, 7, 10, 15, 20, 30, and 50 K for a series of fixed fields, at the wavelengths indicated in the figures.

Spectra were fit to Gaussian band shapes using the program PeakFit (SPSS Science). Saturation magnetization data were normalized to the maximum observed intensity and fit according to published procedures to extract ground-state parameters.[60,61] Application of both negative and positive zero-field splitting models to the VTVH MCD data was used to determine the best fit.

2.4. XAS. X-ray absorption spectra were measured at the Stanford Synchrotron Radiation Laboratory (SSRL) on beam line 9-3 under ring conditions of 50−100 mA and 3 GeV. The optics consisted of an Rh-coated collimating mirror for harmonic rejection, liquid N_2-cooled monochromator (fully tuned), and an Rh-coated post monochromator focusing mirror. The EXAFS data were taken to $k = 15$ Å^{-1} with 1-mm high in-hutch slits. During the measurement, the sample was maintained at 10 K in an Oxford Instruments CF1208 liquid helium flow cryostat. An iron foil standard was used to internally calibrate energies,[62] assigning the first inflection point to 7111.2 eV. The Fe Kα fluorescence data were measured using a 30-element Ge solid-state array detector with a three-wavelength Mn filter and Soller slits. During data reduction, sets of four successive scans were averaged and compared to the previous averages. No change in the edge or EXAFS data was observed over time; thus the final, averaged data set included all 29 scans. Reduction and normalization of the averaged data were performed according to established methods.[62−65] A smooth preedge background was removed from the averaged spectra by fitting a Gaussian function to the preedge region and subtracting this function from the entire spectrum. A three-segmented spline approximately even in *k*-space was fit to the EXAFS region, and the data were normalized to an edge jump of one at 7130 eV.

The intensities and energies of the preedge features of the sample were quantified by least-squares fits of pseudo-Voigt line shapes to the data (half-Gaussian, half-Lorentzian peaks) using the fitting program EDG_FIT[66] as described elsewhere.[67] The total preedge area and peak energies were obtained as a result of nine successful fits that reproduced the data and the second derivative of the data over the entire fit range.

On the basis of the model depicted in Supporting Information Figure S3, theoretical EXAFS phase and amplitude functions were calculated by FEFF (version 6). Least-squares EXAFS fits were performed using EXAFSPAK.[68] Absorber−scatterer distances (Å) and Debye−Waller factors (σ^2 in Å^2) were allowed to float in all fits. The threshold energy in eV ($k = 0$, E_0) was kept to a common variable (ΔE_0) value relative to 7130 eV for all components within a given fit of a sample. Fits were evaluated by comparing the normalized error for each fit, *F*, and

(59) Browett, W. R.; Fucaloro, A. F.; Morgan, T. V.; Stephens, P. J. *J. Am. Chem. Soc.* **1983**, *105*, 1868−1872.

(60) Solomon, E. I.; Pavel, E. G.; Loeb, K. E.; Campochiaro, C. *Coord. Chem. Rev.* **1995**, *144*, 369−460.

(61) Pavel, E. G.; Kitajima, N.; Solomon, E. I. *J. Am. Chem. Soc.* **1998**, *120*, 3949−3962.

(62) Scott, R. A.; Hahn, J. E.; Doniach, S.; Freeman, H. C.; Hodgson, K. O. *J. Am. Chem. Soc.* **1982**, *104*, 5364−5369.

(63) Cramer, S. P.; Hodgson, K. O. *Prog. Inorg. Chem.* **1979**, *25*, 1−39.

(64) DeWitt, J. G.; Bentsen, J. G.; Rosenzweig, A. C.; Hedman, B.; Green, J.; Pilkington, S.; Papaefthymiou, G. C.; Dalton, H.; Hodgson, K. O.; Lippard, S. J. *J. Am. Chem. Soc.* **1991**, *113*, 9219−9235.

(65) Zhang, H. H.; Hedman, B.; Hodgson, K. O. In *Inorganic Electronic Structure and Spectroscopy*; Solomon, E. I., Lever, A. B. P., Eds.; John Wiley & Sons: New York, 1999; pp 513−554.

(66) George, G. N.; EDG_FIT.; Stanford Synchrotron Radiation Laboratory, Stanford Linear Accelerator Center, Stanford University, Stanford, CA 94309.

(67) Westre, T. E.; Kennepohl, P.; DeWitt, J. G.; Hedman, B.; Hodgson, K. O.; Solomon, E. I. *J. Am. Chem. Soc.* **1997**, *119*, 6297−6314.

(68) George, G. N. EXAFSPAK.; Stanford Synchrotron Radiation Laboratory, Stanford Linear Accelerator Center, Stanford University, Stanford, CA 94309.

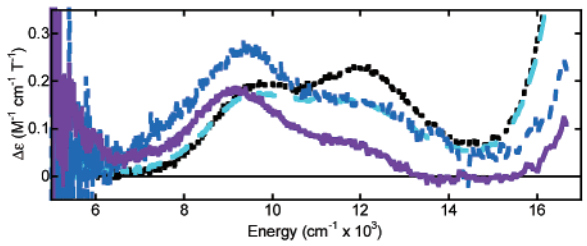

Figure 2. MCD spectra taken at 5 K and 7 T of Fe^{II}BLM complexed with ctDNA: 8 base pairs/BLM in cyan (− −); 20 base pairs/BLM in blue (- - -); 30 base pairs/BLM in purple (—). The spectrum of Fe^{II}BLM (no DNA) is shown in black (···), replotted using data from ref 50.

by visual inspection of the fits to the EXAFS data and the respective Fourier transforms. Since EXAFS cannot distinguish between backscatterers of $Z \pm 1$, all first coordination sphere components were fit with nitrogen phases and amplitudes. More distant second-shell single scattering and multiple scattering waves were fit with carbon and nitrogen components calculated by FEFF. While the total first-shell coordination number for Fe was obtained from preedge analysis and kept constant in the EXAFS fits, the distribution of ligands into shorter or longer components was varied in integer steps to determine the best fit.

2.5. EPR Spectroscopy. EPR spectra were obtained using a Bruker EMX spectrometer, ER 041XG microwave bridge, and ER 4102ST cavity. All samples were run at 77 K in a liquid nitrogen finger Dewar at a frequency of 9.40 GHz.

3. Results and Analysis

3.1. Fe^{II}BLM with Calf Thymus DNA. The ^5D ground state for the d^6 Fe^{II} free ion is split under octahedral symmetry into a $^5T_{2g}$ ground state (d_{xz}, d_{yz}, d_{xy}) and a ^5E_g excited state (d_{z^2}, $d_{x^2-y^2}$), separated by $10Dq \approx 10\,000$ cm^{-1} for oxygen and nitrogen ligands. The splitting of the ^5E_g excited state, Δ^5E_g, is sensitive to the coordination number and geometry of the Fe^{II} site, and transitions to these orbitals can be observed in near-IR CD and MCD spectroscopy.[60,69,70] Model studies have shown that six-coordinate (6C) distorted octahedral Fe^{II} sites have two transitions centered at ~10 000 cm^{-1} with $|\Delta^5E_g| \approx 2000$ cm^{-1}, five-coordinate (5C) sites have two transitions at ~10 000 cm^{-1} and ~5000 cm^{-1} with $|\Delta^5E_g| \approx 5000$ cm^{-1}, and four-coordinate (4C) sites have two transitions in the region of 4000−7000 cm^{-1}.[61] For 5C sites, the two transitions shift from higher to lower energy as the geometry changes from square pyramidal to trigonal bipyramidal.

The near-IR ligand field spectrum of Fe^{II}BLM is shown in black in Figure 2 and has been previously resolved into two transitions at 9410 and 12 050 cm^{-1}, consistent with a distorted octahedral Fe^{II} site.[50] The splitting of Δ^5E_g by >2000 cm^{-1} indicates an axial ligand is weak at the sixth site. The corresponding spectra of Fe^{II}BLM complexed with ctDNA are displayed for increasing concentrations: 8 base pairs/BLM molecule (cyan), 20 base pairs/BLM (blue), and 30 base pairs/BLM (purple). At the lowest concentration of calf thymus DNA, the intensity ratio of the d → d transitions is reversed, and the intensity of the higher energy band continues to decrease as DNA concentration increases. Thus there is a large perturbation of the Fe^{II} site upon DNA binding at >20 base pairs/BLM.

Gaussian analysis of the Fe^{II}BLM+ctDNA spectrum at 30 base pairs/BLM shows that there are two bands at 9100 cm^{-1} and 11 420 cm^{-1}, with a smaller Δ^5E_g splitting relative to Fe^{II}BLM without DNA (Table 1 and Supporting Information Figure S4A). The change in d-orbital transition energies would affect orbital mixing, leading to the change in intensity ratio observed for the two bands. These parameters are consistent with a 6C Fe^{II} site that has a stronger axial ligand relative to Fe^{II}BLM (no DNA). At the highest concentration, an additional small feature is observed at ~5000 cm^{-1}. This feature is attributed to a small amount of oxidation in the sample; Fe^{III}BLM (no DNA) exhibits a similar low-energy feature.[71] Although EPR studies of Fe^{II}BLM−NO have indicated that a 40 base pair/BLM ratio is required for complete perturbation,[44] it was not feasible for MCD studies to exceed 30 base pair/BLM due to solubility difficulties with ctDNA at the high Fe^{II} concentrations required. Consequently, a full MCD spectral perturbation may not be observed, even in the 30 base pairs/BLM sample.

3.2. Fe^{II}BLM with DNA Oligonucleotides. 3.2.1. MCD Spectroscopy. Due to the difficulty of working with ctDNA at high concentrations, DNA oligonucleotides were used to investigate the nature of the Fe^{II}BLM−DNA interaction in more detail. The near-IR MCD spectra of Fe^{II}BLM complexed with two oligonucleotides, d(GGAAGCTTCC)$_2$ (DNA_{GC}) and d(GGAAATTTCC)$_2$ (DNA_{ns}), are shown in Figure 3. These oligomers were chosen because their sequences are identical except for the center oligonucleotides: the DNA_{GC} oligomer contains a 5′-GC-3′ preferred cleavage site, while the DNA_{ns} oligomer has a nonspecific (ns) 5′-AT-3′ sequence in its place. Their interactions with BLM have also been investigated using other methods.[31,37,45−47]

The spectra of Fe^{II}BLM+DNA_{GC} or +DNA_{ns} both show the same perturbation seen in Fe^{II}BLM+ctDNA, with a change in the intensity ratio of the transitions and a smaller Δ^5E_g, indicative of a stronger axial ligand in a 6C Fe^{II} site (Table 1 and Supporting Information Figure S4B,C). Several other oligomers were investigated (Supporting Information Figures S5−S9), and the spectra of those Fe^{II}BLM+DNA complexes are qualitatively similar, although the perturbation is dependent on oligomer length and composition. There is also some spectroscopic variability in the DNA_{ns} samples that appears to be dependent on the oligonucleotide sample used in a particular preparation (Supporting Information Figure S10). Eight samples each of Fe^{II}BLM+DNA_{GC} or +DNA_{ns} have been analyzed, two with unpurified and six with purified DNA. All Fe^{II}BLM+DNA_{GC} samples showed a perturbation similar to that shown in Figure 3A (purple). Although early spectra of Fe^{II}BLM+DNA_{ns} were similar to resting Fe^{II}BLM (Supporting Information Figure S10), the final three samples, all with purified DNA, have consistently shown the full perturbation as depicted in Figure 3 (green). It should be noted that a number of variables may lead to unperturbed spectra through incomplete binding or sample degradation; a change in the MCD spectrum suggests that nonspecific oligomer binding perturbs the metal environment in Fe^{II}BLM.

The temperature and field dependence of the d → d transitions observed by MCD are characterized by the nesting (nonsuperimposing behavior) of isotherms when intensity is plotted vs

(69) Solomon, E. I.; Brunold, T. C.; Davis, M. I.; Kemsley, J. N.; Lee, S.-K.; Lehnert, N.; Neese, F.; Skulan, A. J.; Yang, Y.-S.; Zhou, J. *Chem. Rev.* **2000**, *100*, 235−349.
(70) Solomon, E. I. *Inorg. Chem.* **2001**, *40*, 3656−3669.
(71) Neese, F.; Zaleski, J. M.; Loeb Zaleski, K.; Solomon, E. I. *J. Am. Chem. Soc.* **2000**, *122*, 11703−11724.

Table 1. Ligand Field Transition Energies and Ground-State Parameters

	band 1[a]	band 2[a]	$10D_q$[a]	Δ^5E_g[a]	δ[a]	$g_{\|\|}$	Δ[a]	$\|V\|$[a]
Fe^{II}BLM[b]	9410	12 050	10 730	2640	2.4	9.6	−450	120
Fe^{II}BLM+ctDNA	9100	11 420	10 260	2320				
Fe^{II}BLM+DNA$_{GC}$	9090	10 480	9780	1390	3.1	9.4	−400	120
Fe^{II}BLM+DNA$_{ns}$	9140	11 240	10 140	2100	2.3	9.5	−500	120
Fe^{II}*iso*-PEPLM[c]	8700	11 680	10 190	2980	4.8	9.0	−600	380
Fe^{II}*iso*-PEPLM+DNA$_{GC}$	*mixture of species similar to Fe^{II}iso-PEPLM and Fe^{II}BLM+DNA$_{GC}$*							
Fe^{II}DP-PEPLM[c]	8000	12 200	10 100	4200	4.4	9.2	−600	240
Fe^{II}DP-PEPLM+DNA$_{GC}$	7610	12 240	9925	4630	3.6	8.9	−200	70
					4.2	8.8	−150	60

[a] Values in cm^{-1}. [b] Data from ref 50 refit. [c] Values taken from ref 51.

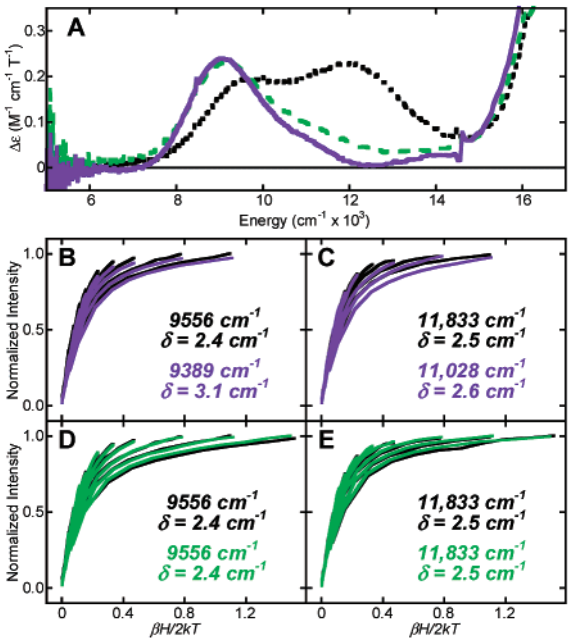

Figure 3. (A) MCD spectra taken at 5 K and 7 T of Fe^{II}BLM+DNA$_{GC}$ in purple (—), Fe^{II}BLM+DNA$_{ns}$ in green (− −), and Fe^{II}BLM in black (···). (B−C) VTVH MCD data for Fe^{II}BLM+DNA$_{GC}$ in purple and Fe^{II}BLM in black. (D−E) VTVH MCD data for Fe^{II}BLM+DNA$_{ns}$ in green and Fe^{II}BLM in black. Data were fit according to the parameters in Table 1. Error bars are approximately twice the line width. Fe^{II}BLM data are replotted from ref 50.

$\beta H/2kT$ and can be used to gain insight into the ground-state electronic structure of Fe^{II} sites.[60,69,70] For systems with negative zero-field splitting (−ZFS; $D < 0$) this behavior is due to the rhombic zero-field splitting (δ) of the $M_S = \pm 2$ doublet ground state. Ground-state parameters are obtained by computationally fitting the experimental VTVH MCD data to an orientation-averaged intensity expression that includes the rhombic and Zeeman splitting of a non-Kramers doublet (δ and $g_{||}$) as well as the transition polarization ratio (M_z/M_{xy}) and contributions from linear temperature-independent ***B***-terms and low-lying excited states.[60,69,70] The results obtained from this analysis are directly related to the splitting of the $^5T_{2g}$ ground state such that the orbital splittings may be determined ($\Delta \equiv d_{xz,yz} - d_{xy}$; $V \equiv d_{xz} - d_{yz}$).

The VTVH data for Fe^{II}BLM+DNA$_{GC}$ (purple) or +DNA$_{ns}$ (green) are shown in Figure 3, parts B−E, overlaid with data for Fe^{II}BLM (black) for reference. As can be seen in parts B and D, the nesting of the +DNA data at ∼9500 cm^{-1}, regardless of sequence, is nearly identical to that for resting Fe^{II}BLM and fits with similar parameters, yielding d-orbital splittings of $\Delta \approx -450$ cm^{-1} and $|V| = 120$ cm^{-1} (Table 1). This indicates that although the energies of the e-symmetry orbitals change upon DNA binding, the t_2 orbitals are not similarly affected. At higher energy, the +DNA$_{ns}$ data overlay that for Fe^{II}BLM (Figure 3E) but the Fe^{II}BLM+DNA$_{GC}$ data appear to have somewhat greater nesting (Figure 3C). The data in this region, however, are at significantly lower intensity, and the difference in nesting is not outside of error. The data fit with a similar δ and have the same ground-state orbital splittings and thus are considered consistent with the data obtained for the lower-energy band.

The ligand-field MCD data from all DNA-bound samples, including both ctDNA (Figure 2) and oligonucleotides (Figure 3, Supporting Information Figures S5−S10), indicate that the spectra observed for Fe^{II}BLM+DNA samples are a mixture of two components. One species is the Fe^{II} site seen for resting Fe^{II}BLM without DNA, in which the two d → d transitions have similar intensity (Figure 3A, black). The other species is the full Fe^{II}BLM−DNA interaction, in which the higher-energy d → d band has lost significant intensity, as represented by Fe^{II}BLM+ctDNA at 30 base pairs/BLM (Figure 2, purple) and Fe^{II}BLM+DNA$_{GC}$ (Figure 3A, purple). All DNA-bound forms are considered to be mixtures of these two limiting species, with the actual composition dependent on sample preparation, concentration, oligomer length, and/or oligomer sequence. Because the spectrum of Fe^{II}BLM+DNA$_{GC}$ is most perturbed, matches the high-concentration Fe^{II}BLM+ctDNA spectrum most closely, and has similar saturation nesting over both d → d bands, it is considered to be representative of the Fe^{II}BLM−DNA interaction and is the focus of further study. Overall, Fe^{II}BLM+DNA$_{ns}$ ligand-field MCD spectra show less of an effect—that is, more Fe^{II}BLM component—but the intensity ratio of the spectrum in Figure 3A clearly shows that the Fe^{II}BLM−DNA species is also present.

The UV/visible MCD spectra for Fe^{II}BLM+DNA$_{GC}$ or +DNA$_{ns}$ are shown in Supporting Information Figure S11A. There is no significant change to the charge-transfer bands for these species as compared to those for Fe^{II}BLM, demonstrating that the hydrogen-bonding interaction of the pyrimidine ring to the guanine of the preferred cleavage site has no effect on the iron site.

3.2.2. XAS. Preedge Analysis. The preedge features that arise due to 1s → 3d transitions can also provide information on the coordination number and geometry of the Fe active site.[67] Since the 1s → 3d transition is formally electric dipole forbidden, it gains its intensity from the ∼100-fold weaker electric quadrupole mechanism. Typical preedges of 6C (octahedral) ferrous complexes are broad and flat with total normalized areas of ∼4

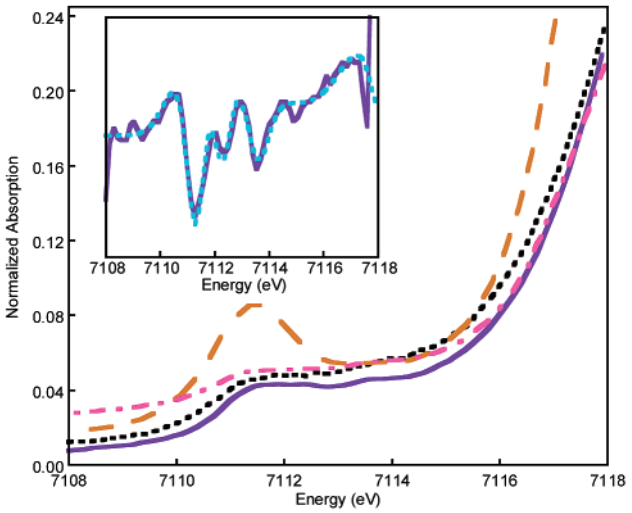

Figure 4. Preedge spectra of $Fe^{II}BLM+DNA_{GC}$ in purple (—), $Fe^{II}BLM$ in black (···), the 6C model complex $[Fe(Im)_6]Cl_2$ in pink (- - -), and the 5C model complex $[Fe(TMC)Cl](BF_4)$ in orange (— —). Inset shows the second derivative of the $Fe^{II}BLM+DNA_{GC}$ spectrum (purple, —) and the fit to the second derivative (cyan, - - -).

Table 2. Preedge Energies and Intensities

	preedge peak energy (eV)[a]	peak intensity[a,b]	total intensity[b]
$Fe^{II}BLM+DNA_{GC}$	7111.36 (0.04)	3.0 (0.4)	
	7112.34 (0.06)	1.6 (0.1)	6.8 (0.2)
	7113.56 (0.05)	2.2 (0.4)	
$Fe^{II}BLM$[c]	7111.26 (0.05)	3.2 (0.3)	
	7112.24 (0.08)	1.8 (0.4)	7.5 (0.3)
	7113.62 (0.05)	2.5 (0.2)	
$[Fe(Im)_6]Cl_2$[d]	7111.24 (0.03)	1.6 (0.5)	3.8 (0.3)
	7112.35 (0.16)	1.6 (0.8)	
	7113.66 (0.02)	0.6 (0.2)	
$[Fe(TMC)Cl](BF_4)$[d]	7111.41 (0.01)	10.9 (0.1)	12.9 (0.2)
	7113.43 (0.02)	2.0 (0.3)	

[a] Values in parentheses are standard deviations for the measured quantities, over three fitting ranges. [b] Values multiplied by 100. [c] Data from ref 50 refit. [d] Data from ref 67.

units distributed over three features, split by approximately 2 eV. In 5C and nonplanar 4C complexes, the center of inversion is eliminated, thus allowing the iron 4p orbitals to mix into the unoccupied and half-occupied 3d orbitals. Since the 1s → 4p transition is electric dipole allowed, only a few percent 4p mixing is necessary to greatly enhance the intensity of the preedge feature. Noncentrosymmetric complexes are therefore observed to have a higher preedge intensity; 5C and tetrahedral ferrous models are fit well by two features having totals of ∼12 and ∼13 units of intensity, respectively.[67]

The preedge spectra of $Fe^{II}BLM+DNA_{GC}$, $Fe^{II}BLM$,[50] $[Fe(Im)_6]Cl_2$ (Im = imidazole), and $[Fe(TMC)Cl](BF_4)$ (TMC = 1,4,8,11-tetramethyl-1,4,8,11-tetraazacyclotetradecane) are shown in Figure 4, and the intensities and energies for the preedge features are listed in Table 2. The overall shape and intensity distribution of the preedge spectrum of $Fe^{II}BLM+DNA_{GC}$ are extremely similar to those of the 6C model complex $[Fe(Im)_6]Cl_2$ and $Fe^{II}BLM$, and it is much less intense and of different shape than the preedge spectrum of the 5C complex $[Fe(TMC)Cl](BF_4)$.

The preedge data and second derivative of the $Fe^{II}BLM+DNA_{GC}$ data were fit with three features at 7111.36, 7112.34, and 7113.56 eV, giving a total intensity of 6.8 units. Three

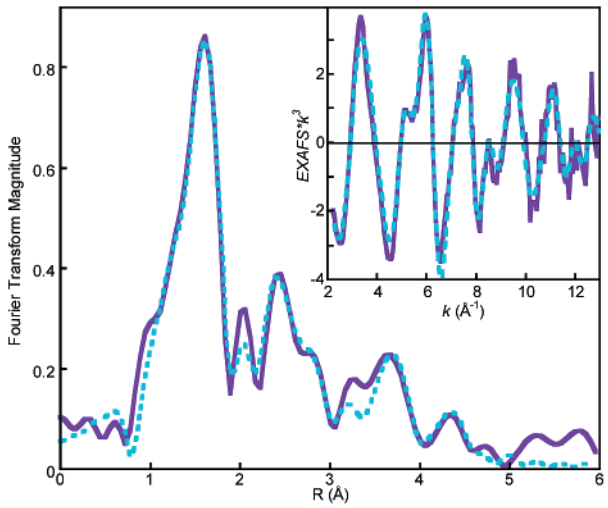

Figure 5. EXAFS analysis for $Fe^{II}BLM+DNA_{GC}$. Fourier transforms of data (purple, —) and fit (cyan, - - -) for $Fe^{II}BLM+DNA_{GC}$. Inset shows EXAFS data (purple, —) and fit to the EXAFS (cyan, - - -).

preedge features at 7111.24, 7112.35, and 7113.66 eV with a total intensity of 3.8 are required to fit the octahedral complex $[Fe(Im)_6]Cl_2$.[67] Therefore, $Fe^{II}BLM+DNA_{GC}$ has a slightly distorted 6C active site with increased preedge intensity equalling ∼2.5% 4p mixing into the Fe 3d orbitals.[67] The 6C $Fe^{II}BLM$ preedge was originally fit with two peaks at ∼7111.5 and ∼7113.5 eV instead of three,[50] as the noise level of the data did not allow resolution of the preedge into three distinct features. For direct comparison with $Fe^{II}BLM+DNA_{GC}$, the preedge data for $Fe^{II}BLM$ were reproduced using three preedge features in the fit (Table 2); and the total intensity obtained as a result of nine fits is 7.5 units, which corresponds to ∼3.0% of 4p mixing into Fe 3d orbitals.[67] Preedge analysis thus shows that upon DNA binding to $Fe^{II}BLM$, less 4p mixing is present in the Fe 3d orbitals and thus the active site becomes a slightly less distorted 6C complex.

EXAFS. The EXAFS data were fit and Fourier transformed over the k range of 2.0−13 $Å^{-1}$, as shown in Figure 5. From the preedge and MCD results, $Fe^{II}BLM+DNA_{GC}$ is 6C; therefore EXAFS fits were performed using a total coordination sphere of six ligands. Modeling the EXAFS data with one nitrogen atom at 1.89 (±0.02) Å and five N/O atoms at 2.08 (±0.02) Å (Table 3, fit 1) gives an adequate fit to the EXAFS data, and good correspondence between the Fourier transforms of the data and fit. Although the σ^2 value of the 1.89-Å component is relatively high, reducing σ^2 up to 40% and floating the remaining parameters does not affect the error value, distances, or the quality of the fit. Thus, the 1.89-Å distance can be considered accurate and the high σ^2 is most likely compensating for a spline-induced low-R feature. The attempt to reproduce the EXAFS fit with only five components in the first shell results in an exceptionally high σ^2 value for the first component (Table 3, fit 2) and confirms the presence of a 6C active site.

The results of EXAFS curve-fitting of $Fe^{II}BLM$ data are discussed in ref 50. For direct correlation with the $Fe^{II}BLM+DNA_{GC}$ EXAFS analysis, $Fe^{II}BLM$ data were refit using the theoretical phase and amplitude parameters calculated by FEFF rather than the previous empirical parameter approach (Supporting Information Figure S12 and Table 3). The six components of the first shell were resolved into the following

Table 3. EXAFS Fits

	fit		CN[a]	*R* (Å)	σ^2 (Å^2)	E_0	*F*[b]
Fe^{II}BLM+DNA$_{GC}$[d]	1	Fe−N	1	1.89	0.00760	−12.3	0.231
		Fe−N/O	5	2.09	0.00751		
		C SS[c]	6	3.00	0.00595		
		N/C MS[c]	16	3.29	0.01163		
		C/N MS[c]	12	4.29	0.00554		
		C/N MS[c]	6	4.75	0.00382		
	2	Fe−N	1	1.96	0.01045	−11.6	0.242
		Fe−N/O	4	2.10	0.00601		
		C SS[c]	6	3.00	0.00588		
		N/C MS[c]	16	3.29	0.01202		
		C/N MS[c]	12	4.30	0.00533		
		C/N MS[c]	6	4.75	0.00380		
Fe^{II}BLM[e]	1	Fe−N	1	1.92	0.00560	−11.6	0.35
		Fe−N/O	5	2.10	0.00599		
		C SS[c]	6	3.00	0.00392		
		N/C MS[c]	16	3.30	0.01150		
		C/N MS[c]	12	4.26	0.00665		

[a] CN = coordination number. [b] $F = \Sigma[(\chi_{exp} - \chi_{obsd})^2 k^6]/\Sigma[\chi_{exp}^2 k^6]$. [c] SS: single scattering, MS: multiple scattering. [d] Fit from $k = 2-13$ Å. [e] Data from ref 50; refit over the range $k = 2-12$ Å.

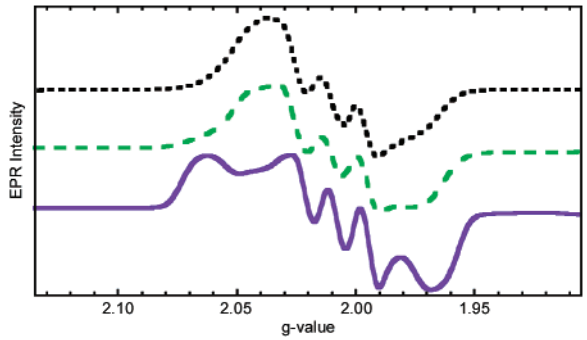

Figure 6. EPR spectra of NO-bound species: ON−Fe^{II}BLM+DNA$_{GC}$ in purple (—), ON−Fe^{II}BLM+DNA$_{ns}$ in green (− −), and ON−Fe^{II}BLM in black (···).

distances: one short component at 1.92 Å with a σ^2 of 0.00560 and five O/N ligands at 2.10 Å ($\sigma^2 = 0.00599$ Å^2). Attempts to locate a first-shell ligand at a distance longer than 2.10 Å, as indicated previously, were unsuccessful. The EXAFS results show that the first shell distances and their distribution in Fe^{II}BLM+DNA$_{GC}$ are, within error, very similar to those of Fe^{II}BLM.

3.2.3 EPR Spectroscopy. Samples studied by MCD were reacted with NO to make the EPR-active {FeNO}^{7} $S = {}^1/_2$ complex[72,73] for comparison to past data on sequence-specific DNA binding effects. The EPR spectra for ON−Fe^{II}BLM, ON−Fe^{II}BLM+DNA$_{GC}$ and ON−Fe^{II}BLM+DNA$_{ns}$ are shown in Figure 6. The spectra show the same effects observed by others using the same DNA oligomers;[45] the spectrum of the Fe^{II}BLM+DNA$_{GC}$ species also mimics that of Fe^{II}BLM+ctDNA.[42−44] In the absence of DNA or with DNA$_{ns}$, the spectrum shows three *g* values; the central resonance has a triplet superhyperfine structure. With ctDNA or DNA$_{GC}$, the *g* values are spread apart into a more rhombic spectrum with little change to the middle *g* value and the superhyperfine splitting. Thus, there appear to be two interactions between FeBLM and DNA. One is a sequence-specific perturbation as observed by EPR in the {FeNO}^{7} complex, while the other is a global DNA binding

(72) Enemark, J. H.; Feltham, R. D. *Coord. Chem. Rev.* **1974**, *13*, 339−406.
(73) Westcott, B. L.; Enemark, J. H. In *Inorganic Electronic Structure and Spectroscopy*; Solomon, E. I., Lever, A. B. P., Eds.; Wiley: New York, 1999; Vol. II, pp 403−450.

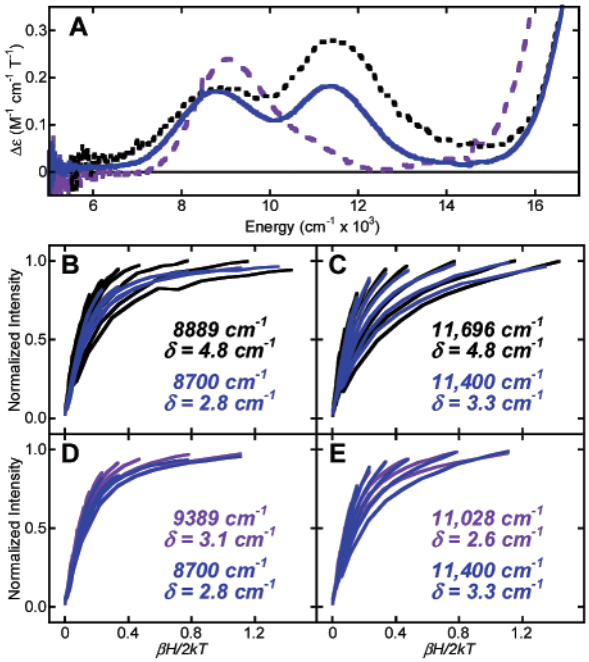

Figure 7. (A) MCD spectra taken at 5 K and 7 T of Fe^{II}*iso*-PEPLM+DNA$_{GC}$ in blue (—), Fe^{II}BLM+DNA$_{GC}$ in purple (− −), and Fe^{II}*iso*-PEPLM in black (···). (B−C) VTVH MCD data for Fe^{II}*iso*-PEPLM +DNA$_{GC}$ in blue and Fe^{II}*iso*-PEPLM in black. (D−E) VTVH MCD data for Fe^{II}*iso*-PEPLM+DNA$_{GC}$ in blue and Fe^{II}BLM+DNA$_{GC}$ in purple. Data were fit according to the parameters in Table 1. Error bars are approximately twice the line width. Fe^{II}*iso*-PEPLM data replotted from ref 51.

effect (not sequence specific) as observed in the MCD spectrum of Fe^{II}BLM with ctDNA, DNA$_{GC}$, and DNA$_{ns}$.

3.3. BLM Derivatives with DNA Oligonucleotides. Because the Fe^{II}BLM+DNA$_{GC}$ complex shows the same spectral change as seen for Fe^{II}BLM+ctDNA, the DNA$_{GC}$ oligonucleotide was used to investigate the DNA binding effects of two BLM derivatives, *iso*-peplomycin and depyruvamide-peplomycin. The difference between BLM and peplomycin (PEPLM) lies in the terminal amine substituent attached to the bithiazole tail (Figure 1), and previous MCD studies have shown no spectral differences between the two structures.[51] The derivative *iso*-PEPLM shifts the carbamoyl substituent on the mannose sugar from the 3- to the 2-hydroxyl group. The depyruvamide (DP)-PEPLM derivative lacks the β-aminoalanine moiety, including the primary amine implicated as an axial ligand to the metal. Both Fe^{II}*iso*-PEPLM and Fe^{II}DP-PEPLM derivatives show significant spectral perturbations relative to Fe^{II}BLM.[51]

3.3.1. Fe^{II}iso-PEPLM+DNA$_{GC}$. The ligand-field MCD spectrum of Fe^{II}*iso*-PEPLM+DNA$_{GC}$ is shown in blue in Figure 7A, with Fe^{II}*iso*-PEPLM (black) and Fe^{II}BLM+DNA$_{GC}$ (purple) shown for reference. The Fe^{II} site in Fe^{II}*iso*-PEPLM+DNA$_{GC}$ is clearly perturbed relative to that in Fe^{II}*iso*-PEPLM, with a change in intensity ratio of the bands and a narrower band at ~9000 cm^{-1} shifted to lower energy. The VTVH MCD data for Fe^{II}*iso*-PEPLM+DNA$_{GC}$ are shown in Figure 7, overlaid with the data for Fe^{II}*iso*-PEPLM (B−C, black) and Fe^{II}BLM+DNA$_{GC}$ (D−E, purple). Different nesting is observed for Fe^{II}*iso*-PEPLM+DNA$_{GC}$ at different wavelengths (blue data in B/D compared to blue data in C/E): the data collected at 11 400 cm^{-1} are much more spread out than the data from 8700 cm^{-1}. This different nesting behavior clearly indicates that the

sample is a mixture of species, since VTVH data arising from a single complex should have the same nesting character across the entire spectrum associated with the presence of only one ground state.

A comparison of the Fe^{II}*iso*-PEPLM+DNA_{GC} VTVH data to that for Fe^{II}*iso*-PEPLM (no DNA; Figure 7B,C) shows that similar nesting is observed for the higher-energy band (C), indicating that a major contribution to this transition is Fe^{II}*iso*-PEPLM. Likewise, comparing the Fe^{II}*iso*-PEPLM+DNA_{GC} data to data for Fe^{II}BLM+DNA_{GC} (Figure 7D,E) shows that the primary component of the lower-energy band (D) is similar to Fe^{II}BLM+DNA_{GC}. These data comparisons indicate that the Fe^{II}*iso*-PEPLM+DNA_{GC} sample appears to be a mixture of two components corresponding to Fe^{II}*iso*-PEPLM and Fe^{II}BLM+DNA_{GC}. Indeed, a composite spectrum of 60% Fe^{II}*iso*-PEPLM plus 40% Fe^{II}BLM+DNA_{GC} closely matches the spectrum of Fe^{II}*iso*-PEPLM+DNA_{GC} (Supporting Information Figure S13). A mixture of species would be consistent with increased stability of the exchangeable ligand in Fe^{II}*iso*-PEPLM relative to that in Fe^{II}BLM, as exhibited through a lower azide-binding constant[51] and reduced DNA cleavage activity.[55−58] Thus, DNA binding produces in Fe^{II}*iso*-PEPLM a species that is the same or very similar to Fe^{II}BLM−DNA, and we can directly link DNA-binding effects to the mannose carbamoyl group. This is consistent with a model in which the carbamoyl provides the sixth, exchangeable ligand to the Fe^{II} and is replaced by solvent when the drug is bound to DNA, or in which carbamoyl second-sphere conformational effects are disrupted by DNA binding.

The charge-transfer MCD spectrum for Fe^{II}*iso*-PEPLM+DNA_{GC} is shown in Supporting Information Figure S11B. As for Fe^{II}BLM, no significant change is observed relative to Fe^{II}*iso*-PEPLM upon DNA binding, indicating that back-bonding to the pyrimidine is not affected.

3.3.2. Fe^{II}DP-PEPLM+DNA_{GC}. Shown in Figure 8A is the spectrum of Fe^{II}DP-PEPLM+DNA_{GC} (red), with Fe^{II}DP-PEPLM (black) and Fe^{II}BLM+DNA_{GC} (purple) for reference. The intensity ratio of the two transitions is roughly the same for Fe^{II}DP-PEPLM+DNA_{GC} as for Fe^{II}DP-PEPLM, with the band at ~8000 cm^{-1} shifted to lower energy. The VTVH MCD data, shown in Figure 8, parts B−E, indicate that the Fe^{II}DP-PEPLM+DNA_{GC} is similar to neither Fe^{II}DP-PEPLM nor Fe^{II}BLM+DNA_{GC}: there is less nesting for Fe^{II}DP-PEPLM+DNA_{GC} (red) relative to Fe^{II}DP-PEPLM (no DNA, parts B−C, black), and more nesting relative to Fe^{II}BLM+DNA_{GC} (parts D,E, purple).

The Fe^{II}DP-PEPLM+DNA_{GC} species also appears to be a mixture, since nesting of the saturation data differs between the two bands (red data in B/D vs C/E). Although the nesting parameter δ varies for different wavelengths, the fit parameters yield similar d-orbital splittings of $\Delta \approx -175$ cm^{-1} and $|V| \approx 65$ cm^{-1} for both bands (Table 1). These splittings are significantly different from those determined for Fe^{II}DP-PEPLM (no DNA) and contrasts with the effect seen for Fe^{II}BLM, in which the energies of the t_2 orbitals do not change upon DNA binding. The formation of a new species with Fe^{II}DP-PEPLM +DNA_{GC} would be consistent with the combined effects of replacing the axial primary amine ligand (due to loss of the primary amine ligand) as well as disruption of the sixth, exchangeable ligand (due to DNA binding), as seen for Fe^{II}BLM and Fe^{II}*iso*-PEPLM.

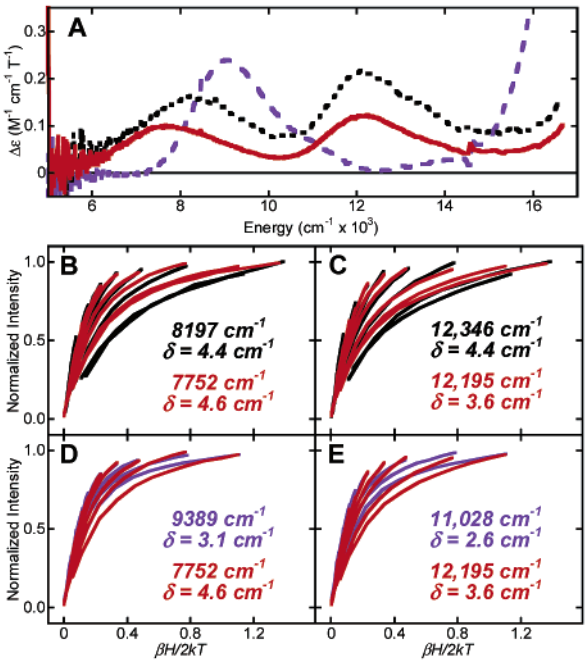

Figure 8. (A) MCD spectra taken at 5 K and 7 T of Fe^{II}DP-PEPLM+DNA_{GC} in red (—), Fe^{II}BLM+DNA_{GC} in purple (− −), and Fe^{II}DP-PEPLM in black (···). (B−C) VTVH MCD data for Fe^{II}DP-PEPLM+DNA_{GC} in red and Fe^{II}DP-PEPLM in black. (D−E) VTVH MCD data for Fe^{II}DP-PEPLM+DNA_{GC} in red and Fe^{II}BLM+DNA_{GC} in purple. Data were fit according to the parameters in Table 1. Error bars are approximately twice the line width. Fe^{II}DP-PEPLM data replotted from ref 51.

The charge-transfer MCD spectrum for Fe^{II}DP-PEPLM+DNA_{GC} is shown in Supporting Information Figure S11C. As for Fe^{II}BLM and Fe^{II}*iso*-PEPLM, no significant change is observed relative to Fe^{II}DP-PEPLM, indicating that the weakened pyrimidine interaction induced by the DP structure is not affected by DNA binding.

3.4. Azide Binding Studies. MCD studies were pursued for azide-bound forms of Fe^{II}BLM and the derivatives to evaluate the effects of DNA binding on the interaction of small molecules with the catalytically relevant Fe^{II} active site. Figure 9A shows the spectrum of N_3^-−Fe^{II}BLM+DNA_{GC} in pink, with N_3^-−Fe^{II}BLM (black) and Fe^{II}BLM+DNA_{GC} (purple) for reference. The azide-bound forms are identical, regardless of whether DNA is present, indicating that the Fe^{II} ligand set is the same in the two species.

The binding constants for azide to Fe^{II}BLM+DNA_{GC} and +DNA_{ns} were determined through CD spectroscopy. Figure 10 shows the spectra for Fe^{II}BLM+DNA_{GC} upon the addition of 0, 5, 10, 30, 63, and 97 equiv of N_3^-. The original spectrum with two positive CD bands changes to a new spectrum with one positive and one negative band, as observed for Fe^{II}BLM (Supporting Information Figure S14A and ref 51). The reaction appears to be complete by 63 equiv of N_3^-. Similar results are observed for Fe^{II}BLM+DNA_{ns} (Supporting Information Figure S14B). A Scatchard analysis[74] of the titration data yields azide binding constants of 7 ± 3 M^{-1} for Fe^{II}BLM+DNA_{GC} and 5 ± 4 M^{-1} for Fe^{II}BLM+DNA_{ns}, indicating that within error the two oligomer-bound species have the same affinity

(74) Fersht, A. *Enzyme Structure and Mechanism*, 2nd ed.; W. H. Freeman and Company: New York, 1985; pp 190−191.

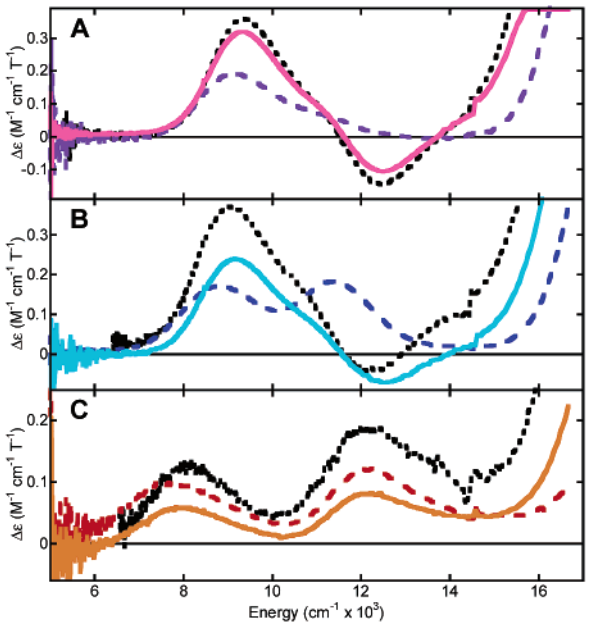

Figure 9. MCD spectra taken at 5 K and 7 T: (A) N_3^-−Fe^{II}BLM+DNA$_{GC}$ in pink (—), Fe^{II}BLM+DNA$_{GC}$ in purple (− −), and N_3^-−Fe^{II}BLM in black (···); (B) N_3^-−Fe^{II}*iso*-PEPLM+DNA$_{GC}$ in cyan (—), Fe^{II}*iso*-PEPLM+DNA$_{GC}$ in blue (− −), and N_3^-−Fe^{II}*iso*-PEPLM in black (···); (C) N_3^-−Fe^{II}DP-PEPLM+DNA$_{GC}$ in orange (—), Fe^{II}DP-PEPLM+DNA$_{GC}$ in red (− −), and N_3^-−Fe^{II}DP-PEPLM in black (···). N_3^-−Fe^{II}BLM, N_3^-−Fe^{II}*iso*-PEPLM, and N_3^-−Fe^{II}DP-PEPLM data replotted from ref 51.

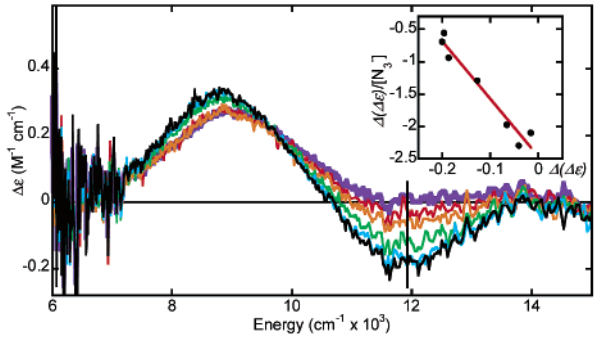

Figure 10. CD spectra taken at 298 K for azide titration to Fe^{II}BLM+DNA$_{GC}$: 0 equiv N_3^-, purple; 5, red; 10, orange; 30, green; 63, cyan; 97, black. Data for 0.5, 1, 2, and 120 equiv N_3^- are not shown for clarity. Inset shows Scatchard plot of data collected at 11 933 cm^{-1} (at vertical line in spectra); data for 0.5 and 1 equiv N_3^- were not included in Scatchard analysis because of large errors in low-intensity data. [Unpurified oligomers from Operon.]

for N_3^-. The DNA-bound species have a significantly lower affinity for N_3^- than Fe^{II}BLM alone (33 ± 3 M^{-1}, Supporting Information Figure S14).[51,75] This is consistent with previous results demonstrating that azide dissociates from Fe^{III}BLM upon binding of ctDNA.[38]

The spectrum of N_3^-−Fe^{II}−*iso*-PEPLM+DNA$_{GC}$ is shown in cyan in Figure 9B, as well as N_3^-−Fe^{II}*iso*-PEPLM (black) and Fe^{II}*iso*-PEPLM+DNA$_{GC}$ (blue). As seen for Fe^{II}BLM, the azide-bound spectra are nearly identical in the presence and absence of DNA. Comparing these data to those for N_3^-−Fe^{II}BLM, we note that all four species—N_3^-−Fe^{II}BLM, N_3^-−Fe^{II}BLM+DNA$_{GC}$, N_3^-−Fe^{II}*iso*-PEPLM, and N_3^-−Fe^{II}*iso*-PEPLM+DNA$_{GC}$—show qualitatively similar spectra and therefore must have equivalent first-coordination sphere environments. This would again be consistent with a model in which there are six endogenous ligands to the Fe^{II}, with carbamoyl as the sixth, exchangeable ligand that can be replaced by solvent (if DNA is present) or azide.

Figure 9C shows the spectrum of N_3^-−Fe^{II}DP-PEPLM+DNA$_{GC}$ in orange, N_3^-−Fe^{II}DP-PEPLM in black, and Fe^{II}DP-PEPLM+DNA$_{GC}$ in red. In this case, azide binding to the Fe^{II} does not significantly alter the spectrum relative to Fe^{II}DP-PEPLM+DNA$_{GC}$, and the spectra continue to be unique relative to those of the Fe^{II}BLM and Fe^{II}*iso*-PEPLM species.

4. Discussion

The interactions of BLM with ctDNA and oligonucleotides have been extensively studied as a means to understand the unique sequence-selective, single- and double-strand DNA cleavage activity of BLM. Most of those investigations, however, have focused on metal-substituted or exogenous ligand-bound forms of the drug and do not directly address the properties and activity of the drug in vivo. The MCD, VTVH MCD, and XAS methodologies we have developed allow us to directly probe the catalytically relevant Fe^{II} site. Our previous studies concerning Fe^{II}BLM and selected structural derivatives have demonstrated that the active site is 6C, most likely with six endogenous ligands including the primary amine of the β-aminoalanine and the carbamoyl of the mannose sugar.[50−52] Alternatively, if the ligand wrap proposed for HOO−Co^{III}BLM is appropriate for the Fe^{II} complex,[21] the carbamoyl group must be involved in a significant second-sphere interaction that directly affects the Fe^{II} site. Low-energy charge-transfer transitions were correlated with Fe^{II} $d_\pi \rightarrow$ pyrimidine π^* back-bonding.

We have now extended those studies to investigate the interaction of Fe^{II}BLM with its substrate, DNA. MCD spectra of Fe^{II}BLM+ctDNA show that the presence of substrate perturbs the ligand structure of the metal at a ratio as low as eight base pairs/BLM. This effect becomes more pronounced as the relative amount of DNA to BLM is increased. The change in intensity ratio of the d → d bands and decrease in Δ^5E_g observed in the ctDNA complex is also seen when Fe^{II}BLM is bound to DNA oligonucleotides, including either DNA$_{GC}$ or DNA$_{ns}$. The energy-level diagram in Figure 11 derived from the MCD data shows the change in d-orbital energies upon DNA binding, going from Fe^{II}BLM in the first column (black) to Fe^{II}BLM+DNA in the second column (purple). XAS preedge and EXAFS analyses confirm that the DNA-bound form is 6C, and the observed reduction in preedge intensity for Fe^{II}BLM+DNA$_{GC}$ is consistent with a stronger axial interaction also indicated by a reduced Δ^5E_g energy splitting. No effects are observed in the charge-transfer transitions arising from back-bonding to the pyrimidine ring, indicating that a sequence-specific H-bonding interaction between the pyrimidine and a guanine base has no effect on the Fe^{II} site. Azide-binding studies demonstrate that, within error, the Fe^{II}BLM+DNA$_{GC}$ and +DNA$_{ns}$ species have the same affinity for N_3^-.

Further MCD studies investigating the effects of BLM structural derivations indicate that DNA binding produces the same effect on Fe^{II}*iso*-PEPLM as for Fe^{II}BLM, as shown in Figure 11 going from Fe^{II}*iso*-PEPLM in the third column (black) to the DNA bound form in the second column (purple). Azide-

(75) The difference between azide binding constants for Fe^{II}BLM in this paper and the one reported previously is due to temperature: 298 K in this work and 278 K in ref 51.

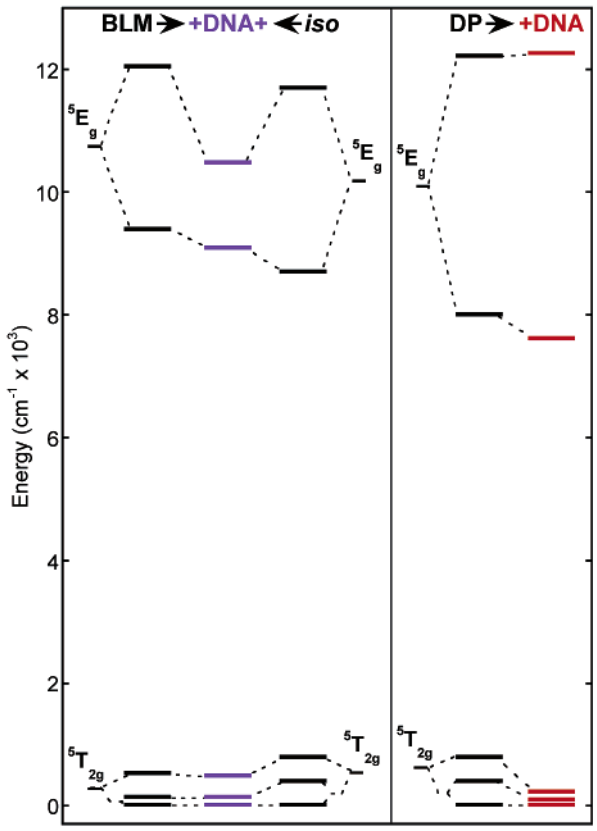

Figure 11. Experimentally determined d-orbital energy levels for Fe^{II}BLM (first column, black), Fe^{II}BLM+DNA_{GC} and Fe^{II}*iso*-PEPLM+DNA_{GC} (second column, purple), Fe^{II}*iso*-PEPLM (third column, black), Fe^{II}DP-PEPLM (fourth column, black), and Fe^{II}DP-PEPLM+DNA_{GC} (fifth column, red).

binding studies further show that the N_3^-−Fe^{II}BLM and N_3^-−Fe^{II}*iso*-PEPLM species are the same in the presence and absence of DNA. In contrast, Fe^{II}DP-PEPLM+DNA_{GC} has a unique spectrum relative to Fe^{II}DP-PEPLM and Fe^{II}BLM+DNA_{GC}. In the case of the DP-PEPLM derivative, the DNA binding effects are more pronounced on the t_2 orbital splittings rather than Δ^5E_g (Figure 11, from the fourth to the fifth column, black to red), in contrast to the changes observed for Fe^{II}BLM and Fe^{II}*iso*-PEPLM. Azide binding has no effect on the MCD spectrum of Fe^{II}DP-PEPLM+DNA_{GC}. As seen for Fe^{II}BLM+DNA, no change in the charge-transfer spectrum is observed for either derivative.

In contrast to other studies that have documented differences in metal−BLM complexes with DNA_{GC} versus DNA_{ns},[45−47,49] the effects observed for the Fe^{II}BLM complex by MCD and XAS are general DNA-binding effects not attributable solely to the presence of a 5′-G-pyrimidine-3′ preferred cleavage site. For these same samples (Fe^{II}BLM+DNA_{GC} and +DNA_{ns}), EPR spectra of the {FeNO}^{7} complexes do show changes specific to the GC site as observed previously.[45] The general interaction observed by MCD is likely due to intercalation of the bithiazole tail, which draws the metal-binding domain into the minor groove of the double helix, creating steric interactions between the DNA and the drug even when sequence-specific H-bonding interactions are not present. The reduced azide-binding constants observed for the DNA-bound species are consistent with a sterically constrained binding pocket. The fact that Fe^{II}BLM and Fe^{II}*iso*-PEPLM have the same MCD spectrum when bound to DNA is consistent with a model in which DNA binding causes a structural perturbation of the sugar domain, removing it from interaction with the exchangeable ligand site. This effect could be due to removal of the carbamoyl oxygen as a ligand in favor of solvent, or removal of a significant second-sphere effect from the carbamoyl group on the Fe^{II} site.

The observation that the Fe^{II}BLM active site is perturbed when bound to nonspecific as well as 5′-GC-3′ sites provides insight into the increased production of DNA cleavage products seen for low concentrations of ctDNA, or for a nonspecific oligomer relative to one with a 5′-GC-3′ sequence.[45,76] The general interaction of Fe^{II}BLM with DNA alters the ligand field of BLM, and it is this species that reacts with O_2 to produce DNA cleavage regardless of binding site. This conclusion would be consistent with increased reactivity observed for Fe^{II}BLM + O_2 when bound to ctDNA.[38] Thus, the sequence-specific cleavage observed for BLM with DNA is likely due to an additional thermodynamic binding component provided by H-bonds between the BLM ligand and the 5′-G-pyrimidine-3′ site,[34−36] rather than an increase in Fe^{II} reactivity induced only by preferred DNA sequences. EPR spectra have also indicated that the structure of activated BLM is not affected by DNA binding, with or without a preferred cleavage sequence.[45] This is consistent with nonsequence specific reactivity, as well as the lack of a DNA binding effect observed for the stabilizing $d_\pi \rightarrow$ pyrimidine π^* metal-to-ligand charge-transfer transitions (Figure S11).

While it has been generally thought that activated BLM proceeds through heterolytic cleavage of the O−O bond to produce a formally Fe^V=O species, recent studies have shown this to be energetically unfavorable since it results in an Fe^{IV}=O species and oxidation of the deprotonated amide ligand, which is difficult.[71] Homolytic cleavage has also been discounted due to the specificity of cleavage and the observed deuterium kinetic isotope effect.[77] Direct H-atom abstraction has been proposed as a concerted version of homolytic cleavage,[78] which should be favorable when the H atom is oriented efficiently toward the peroxide (i.e. with good orbital overlap) since the energy required for O−O cleavage should be compensated by the formation of the O−H bond. The model proposed here, in which the Fe^{II}BLM site has the same structure and therefore the same reactivity regardless of DNA sequence, may indicate a common homolytic cleavage pathway, with direct H-atom abstraction occurring when Fe^{II}BLM is bound at a 5′-G-pyrimidine-3′ site and additional BLM−DNA hydrogen bonds orient activated BLM for C4′−H abstraction.

In summary, we have used MCD and XAS to probe the effects of substrate binding on the biologically relevant Fe^{II}BLM complex. Binding to either ctDNA or oligonucleotides perturbs the Fe^{II} site, resulting in a change in intensity ratio of the d → d transitions, a decrease in the excited-state orbital splitting, and a reduction in preedge intensity, all consistent with a stronger axial ligand interaction. The effects are due to general DNA binding and are not correlated with the presence of a preferred cleavage site. No effect is observed on the charge-

(76) Li, W.; Antholine, W. E.; Petering, D. H. *J. Inorg. Biochem.* **2002**, *90*, 8−17.
(77) Worth, L.; Frank, B. L.; Christner, D. F.; Absalon, M. J.; Stubbe, J.; Kozarich, J. W. *Biochemistry* **1993**, *32*, 2601−2609.
(78) Lehnert, N.; Neese, F.; Ho, R. Y. N.; Que, L., Jr.; Solomon, E. I. *J. Am. Chem. Soc.* **2002**, *124*, 10810−10822.

transfer transitions, indicating that H-bonding recognition between the pyrimidine ligand and guanine base does not affect Fe−pyrimidine back-bonding. Parallel studies on the DP-PEPLM and *iso*-PEPLM derivatives are consistent with a structural model in which the primary amine of the β-aminoalanine and the mannose carbamoyl provide axial ligands to the Fe^{II}; alternatively, the carbamoyl group may provide significant second-sphere effects on the Fe^{II} site. In either case, it is proposed that intercalation of the bithiazole tail into the DNA double helix results in steric interactions with the sugar domain, removing it from interacting with the exchangeable ligand site. The fact that the Fe^{II} active site is perturbed regardless of DNA sequence is consistent with the fact that cleavage is observed for oligomers both with and without preferred cleavage sites, and indicates that different reaction coordinates may be active, depending on orientation of the deoxyribose C4′−H.

Acknowledgment. This work was supported by grants from the National Institutes of Health: GM40392 to E.I.S., RR-01209 to K.O.H., and a Stanford-NIH Biotechnology Training Fellowship to J.N.K. SSRL operations are funded by the U.S. Department of Energy, Office of Basic Energy Science. The Structural Molecular Biology program at SSRL is funded by the National Institutes of Health, National Center for Research Resources, Biomedical Technology Program, and the Department of Energy, Office of Biological and Environmental Research.

Supporting Information Available: Near-IR and visible/UV CD spectra of Fe^{II}BLM+DNA_{GC} and +DNA_{ns}; starting model for FEFF analysis; Gaussian fits for near-IR MCD spectra for Fe^{II}BLM+ctDNA, +DNA_{GC}, and +DNA_{ns}; near-IR MCD spectra of Fe^{II}BLM with other oligonucleotides; near-IR MCD spectra showing variability in Fe^{II}BLM+DNA_{GC} and +DNA_{ns} samples; visible/UV MCD spectra for Fe^{II}BLM+DNA_{GC}, Fe^{II}BLM+DNA_{ns}, Fe^{II}*iso*-PEPLM+DNA_{GC}, and Fe^{II}DP-PEPLM+DNA_{GC}; EXAFS and Fourier transforms of FEFF-based analysis of Fe^{II}BLM; and Fe^{II}*iso*-PEPLM+DNA_{GC} composite spectrum (PDF). This material is available free of charge via the Internet at http://pubs.acs.org.

JA034579N